

MODELING THE EFFECTS OF ALBEDO AND INFRARED RADIATION PRESSURES ON THE MESSENGER SPACECRAFT

Christopher J. Scott,^{*} James V. McAdams,[†] Dawn P. Moessner[‡], and Carl J. Ercol[§]

While the MErcury Surface, Space ENvironment, GEochemistry, and Ranging (MESSENGER) spacecraft is in orbit about Mercury, the navigation team will refine a spherical-harmonic gravity-field model that requires accurate estimation of all perturbing accelerations, including those induced by Mercury's surface albedo and infrared radiation. The incident flux on each spacecraft surface is estimated and converted into perturbing accelerations, which are then incorporated into a propagation model within the Satellite Tool Kit Astrogator module. This paper outlines the calculation and predicted effects of these perturbing accelerations on the MESSENGER spacecraft throughout the mission's orbital phase.

INTRODUCTION

On 18 March 2011, after completing six gravity-assist flybys of inner solar system planets and 17 trajectory correction maneuvers, the MErcury Surface, Space ENvironment, GEochemistry, and Ranging (MESSENGER) spacecraft became the first to orbit Mercury.¹ A spherical-harmonic gravity-field model, to degree and order 20, will be refined by MESSENGER's navigation team at KinetX, Inc., from orbit determination analysis throughout the mission's orbital phase. This gravity model update process requires accurate modeling of the perturbing forces, including solar radiation pressure (SRP) and acceleration induced by planetary albedo and infrared (IR) radiation. This requirement has been demonstrated by modeling for the European Space Agency's BepiColombo Mercury Planetary Orbiter, which showed that albedo radiation has a long-term effect on the orbit, albeit two orders of magnitude less than direct SRP.² This paper summarizes the MESSENGER mission design team's model of the Mercury albedo and IR forces throughout the mission orbital phase based on thermal analyses developed during the design of the spacecraft. These results are used to verify an independent model used by KinetX, Inc.

Mercury's low surface albedo indicates absorption of 75%–94% of the incident solar radiation, resulting in harsh IR thermal environments for orbiters passing close to its surface.³ A bolometric albedo of 0.074 has been assumed for this study.⁴ This surface absorption provides a

^{*} Mission Design Analyst, The Johns Hopkins University Applied Physics Laboratory, 11100 Johns Hopkins Road, Laurel, MD 20723.

[†] Mission Design Lead Engineer, The Johns Hopkins University Applied Physics Laboratory, 11100 Johns Hopkins Road, Laurel, MD 20723.

[‡] Mission Design Analyst, The Johns Hopkins University Applied Physics Laboratory, 11100 Johns Hopkins Road, Laurel, MD 20723.

[§] Thermal Design Lead Engineer, The Johns Hopkins University Applied Physics Laboratory, 11100 Johns Hopkins Road, Laurel, MD 20723.

maximum surface temperature of 430°C at the subsolar point at Mercury perihelion and 297°C at Mercury aphelion.³ The nightside of Mercury has a temperature as low as −180°C, regardless of solar distance. The long, 59-day Mercury rotation period with 3:2 resonance relative to Mercury’s 88-day orbital period supports a steady-state assumption for Mercury surface-temperature distribution over the period of a given orbit. Given an orbit inclination of approximately 83°, the thermal load on the spacecraft was partially attenuated by initially forcing the angle between the subsolar point and the right ascension of the ascending node to be approximately 89° at Mercury perihelion. This orientation corresponds to an orbit that initially lies near the terminator. Thermal modeling of the spacecraft was performed by the MESSENGER thermal design team using the Thermal Radiation Analysis SYStem (TRASYS) software in conjunction with Systems Improved Numerical Differencing Analyzer (SINDA) for 10° increments in Mercury true anomaly. With this thermal model, spacecraft attitude during each orbit follows a set pattern, except during “hot-pole” orientations, which span a range of 80° in Mercury true anomaly. The hot-pole condition is centered about a Sun–Mercury–spacecraft angle of 0° at the orbit’s descending node, which occurs just after periapsis.

Output from this software was passed to the mission design team in the form of incident flux on the spacecraft surfaces, given a reference trajectory produced by the mission design team. The trajectory was produced with a force model that included the most recent 20 × 20 Mercury gravity-field model from the navigation team, the gravitational attraction of all other planets in our solar system, general relativity, and SRP. In addition to Mercury true anomaly, the thermal design team further digitized the data by orbit periapsis altitude and argument of periapsis, with points for the latter quantity at 104°, 106°, 109°, 111°, 114°, 117°, and 119°. The cumulative effect of albedo and IR perturbations on the orbit is small over the yearlong orbital phase. The accelerations resulting from these perturbations on the reference trajectory will be nearly identical to the accelerations experienced on the true trajectory.

A Satellite Tool Kit (STK) Astrogator force plug-in was designed to incorporate the Mercury albedo and IR accelerations on the calculated spacecraft orbit. The flux on the spacecraft surfaces was converted into forces by the mission design team. During orbit propagation, these forces were interpolated on the basis of current position and converted into an acceleration with an estimate of the spacecraft mass. Spacecraft mass changes throughout the orbital mission phase because of the occasional execution of orbit-correction maneuvers and propulsive momentum adjustments. This paper describes the modeling process and the effects of Mercury albedo-IR perturbations on the first Mercury year of MESSENGER’s orbit.

ALBEDO-IR MODEL

The highest non-gravitational acceleration experienced by the MESSENGER spacecraft in its orbital phase will be SRP with order of magnitude about 10^{−7} m/s². This perturbation is subject to seasonal variations as the solar irradiance varies between 14,448 W/m² at Mercury’s perihelion and 6272 W/m² at aphelion. To calculate the albedo-IR force, the surface of Mercury visible to the spacecraft is partitioned into a finite number of elements with area dA . The flux intercepted by an object with cross-sectional area A_c from area element dA can be written as,

$$d\Phi^{\text{Tot}} = d\Phi^{\text{sw}} + d\Phi^{\text{lw}} = (L^{\text{sw}} + L^{\text{lw}}) \frac{A_c}{r^2} dA \cos(\alpha) \quad (1)$$

where L^{sw} and L^{lw} represent the shortwave and longwave, IR, radiance of dA , respectively. Radiance varies with view angle, α , azimuth, and surface properties. These characteristics make precise models difficult to implement numerically.

The spacecraft bus is modeled as six surfaces, i.e., the surfaces perpendicular to spacecraft body axes $\pm x$, $\pm y$, and $\pm z$, and each solar panel comprises two additional surfaces. The thermal team provided the mission design team with albedo and IR flux due to Mercury on each spacecraft surface. In the thermal team's model the temperature distribution across Mercury's surface follows a cosine shape. Mercury's surface is assumed to be 100% emissive and 7% reflective. Fluxes are delivered in units normalized by $I_s = 1360 \text{ W/m}^2$. Thus, the shortwave flux on the $+x$ surface is defined by

$$\Phi_{+x}^{\text{SW}} = \hat{\Phi}_{+x}^{\text{SW}} I_s. \quad (2)$$

The absorptivity, designated as a_{+x} , is also provided by the thermal team. Thus, $(1 - a_{+x})\Phi_{+x}^{\text{SW}}$ represents the portion of the flux that is reflected from the surface for zero transmissivity.

Using Einstein's equation, incoming energy can be related to momentum by

$$p = \frac{E}{c} = \frac{\Phi A \Delta t}{c}, \quad (3)$$

where the flux is assumed to be constant over some timespan Δt . By Newton's second law,

$$F = \frac{dp}{dt} = \frac{\Phi A}{c}. \quad (4)$$

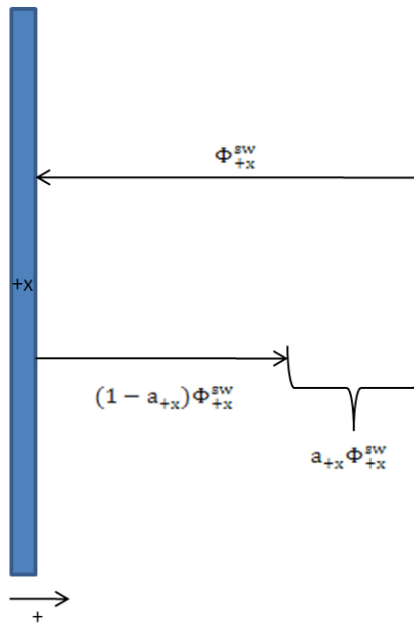


Figure 1. Sketch of Incoming and Outgoing Flux on the $+x$ -Plate.

Summing the momentum over some infinitesimal time shown in Figure 1,

$$\sum dp_{+x}^{\text{SW}} = \left[-\frac{\Phi_{+x}^{\text{SW}} A_{+x}}{c} + \left(-\frac{\Phi_{+x}^{\text{SW}} I_s A_{+x}}{c} (1 - a_{+x}) \right) \right] dt \quad (5)$$

gives

$$f_{+x}^{sw} = \sum \frac{dp_{+x}^{sw}}{dt} = \frac{\hat{\Phi}_{+x}^{sw} I_s A_{+x}}{c} + \frac{\hat{\Phi}_{+x}^{sw} I_s A_{+x}}{c} (1 - a_{+x}) = \frac{\hat{\Phi}_{+x}^{sw} I_s A_{+x}}{c} (a_{+x} - 2). \quad (6)$$

Similarly, for longwave IR radiation, e_{+x} represents the portion of the incoming radiation that is reflected. Thus,

$$f_{+x}^{lw} = \frac{\hat{\Phi}_{+x}^{lw} I_s A_{+x}}{c} (e_{+x} - 2). \quad (7)$$

Letting $+x$ and $-x$, and sw and lw and their corresponding constants, be designated by the indices “j” and “i,” respectively, and letting the x-, y-, and z-directions be designated by the index “k,” each component of the force on the spacecraft bus can be expressed as

$$F_k^{bus} = \sum_{i=1}^2 \sum_{j=1}^2 f_{i,j,k} = \frac{I_s}{c} \sum_{i=1}^2 \sum_{j=1}^2 \hat{\Phi}_{i,j,k} A_{j,k} (C_{i,j,k} - 2) \varepsilon_{j,k} \quad (8)$$

$$\varepsilon_{j,k} = \begin{cases} 1 & j = 1, k = 1, 3 \\ -1 & j = 2, k = 1, 3 \text{ or } j = 1, k = 2 \end{cases} \quad (9)$$

Note that it has been assumed that any absorbed energy is radiated isotropically, generating zero net force on the spacecraft.

The solar panels are pinned along the $\pm x$ -body axes of spacecraft as sketched below in Figure 2.

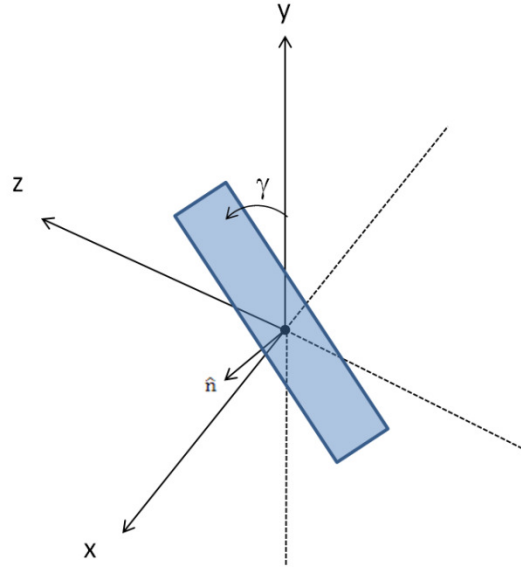


Figure 2. Solar Panel Orientation with Respect to the Spacecraft Body Frame.

The unit vectors normal to the front and back faces of the solar panel attached along the $+x$ -directions are as follows:

$$\hat{\mathbf{n}}_f^{+x} = \begin{bmatrix} 0 \\ -\sin(\gamma^{+x}) \\ \cos(\gamma^{+x}) \end{bmatrix}, \quad \hat{\mathbf{n}}_b^{+x} = -\hat{\mathbf{n}}_f^{+x} \quad (10)$$

Similarly,

$$\hat{\mathbf{n}}_f^{-x} = \begin{bmatrix} 0 \\ -\sin(\gamma^{-x}) \\ \cos(\gamma^{-x}) \end{bmatrix}, \hat{\mathbf{n}}_b^{-x} = -\hat{\mathbf{n}}_f^{-x}. \quad (11)$$

Therefore, the force components due to the solar panels can be expressed as

$$F_k^{\text{SP}} = \sum_{i=1}^2 \sum_{j=1}^2 \sum_{p=1}^2 f_{i,j} \hat{\mathbf{n}}_{j,k,p} = \frac{I_s}{c} \sum_{i=1}^2 \sum_{j=1}^2 \sum_{p=1}^2 \hat{\Phi}_{i,p} A_p (P_{j,p} - 2) \hat{\mathbf{n}}_{j,k,p} \delta_{j,p}, \quad (12)$$

where “k” indicates the component of the force, “j” indicates either the front or back face, “p” indicates the solar panel, and “i” indicates either shortwave or longwave radiation. It is assumed that if a face of the solar panel is not oriented in the direction of the center of Mercury, then its corresponding force is negligible. The unit vector from spacecraft to the center of Mercury is $\hat{\mathbf{u}}_{\varnothing/sc}$. Thus, if $\hat{\mathbf{n}}_j^p \cdot \hat{\mathbf{u}}_{\varnothing/sc} < 0$, then $\delta_{j,p} = 0$.

GEOMETRY AND APPROACH

The albedo-IR fluxes are provided as a function of Mercury year and true anomaly and spacecraft true anomaly. The year is taken to begin at Mercury true anomaly of 0° . These data are interpolated by an STK Astrogator plug-in script providing force as a function of time and geometry. The plug-in was modeled after the SRP plug-in used by the mission design teams for both the MESSENGER and New Horizons spacecraft. Mercury true anomaly is partitioned into discrete increments of 10° , whereas the spacecraft argument of periapsis is partitioned into 104° , 106° , 109° , 111° , 114° , 117° , and 119° . These simplifications are necessary to run the thermal team’s albedo-IR models, yet they introduce errors due to geometry inconsistency when incorporated into a high-fidelity simulation including a precise attitude history. The assumption is that these errors are not large enough to change the qualitative effects of these small forces on the orbit.

Nominal Body Frame

When the spacecraft is not subject to hot-pole constraints, its orientation is determined in the following manner. With the vector from the Sun to the spacecraft in the J2000 frame designated as $\mathbf{r}_{sc/\odot}$, the unit vector from the spacecraft to the Sun is $\hat{\mathbf{u}}_{\odot/sc} = -\mathbf{r}_{sc/\odot}/|\mathbf{r}_{sc/\odot}|$. Similarly, the vector from Mercury to the spacecraft in the J2000 frame, $\mathbf{r}_{sc/\varnothing}$, is used to construct the unit vector from the spacecraft to Mercury, $\hat{\mathbf{u}}_{\varnothing/sc} = -\mathbf{r}_{sc/\varnothing}/|\mathbf{r}_{sc/\varnothing}|$. The three axes of the body frame are

$$\begin{aligned} \hat{\mathbf{i}} &= \hat{\mathbf{u}}_{\varnothing/sc} \times \hat{\mathbf{u}}_{\odot/sc} \\ \hat{\mathbf{j}} &= -\hat{\mathbf{u}}_{\odot/sc} \\ \hat{\mathbf{k}} &= \hat{\mathbf{i}} \times \hat{\mathbf{j}} \end{aligned} \quad (13)$$

and are illustrated in Figure 3. The sunshade points in the $-\hat{\mathbf{j}}$ direction, whereas $\hat{\mathbf{k}}$ points approximately nadir.

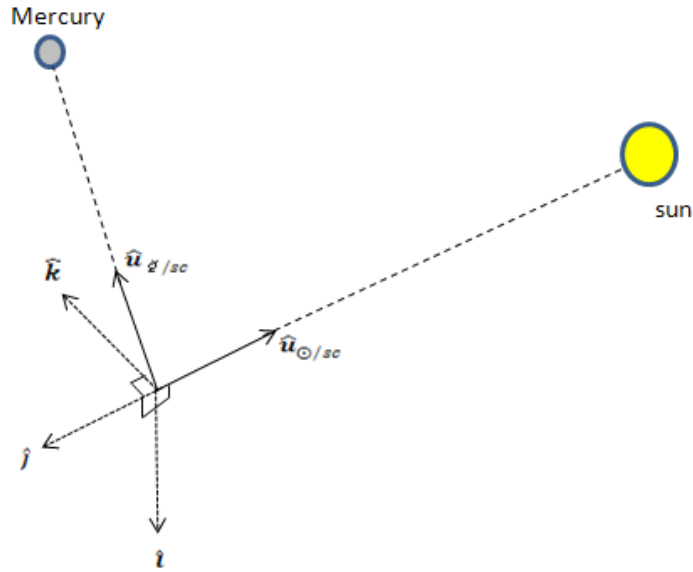


Figure 3. The $\hat{i} - \hat{j} - \hat{k}$ Frame with Respect to Mercury and the Sun. Note That \hat{j} , $\hat{u}_{q/sc}$, and $\hat{u}_{O/sc}$ Lie in the Same Plane.

From the previous developments, the direction cosine matrix relating the body frame to the J2000 frame can be expressed as

$$C_{\text{body}/J2000} = [\hat{i} \quad \hat{j} \quad \hat{k}]. \quad (14)$$

Hot-Pole Orientation

During hot-pole mode, the spacecraft attitude is changed at the equatorial crossings to help attenuate an intensified thermal environment. This situation occurs at spacecraft true anomaly values of approximately 60° and 240° . For the nominal science orbit, see Figure 4.

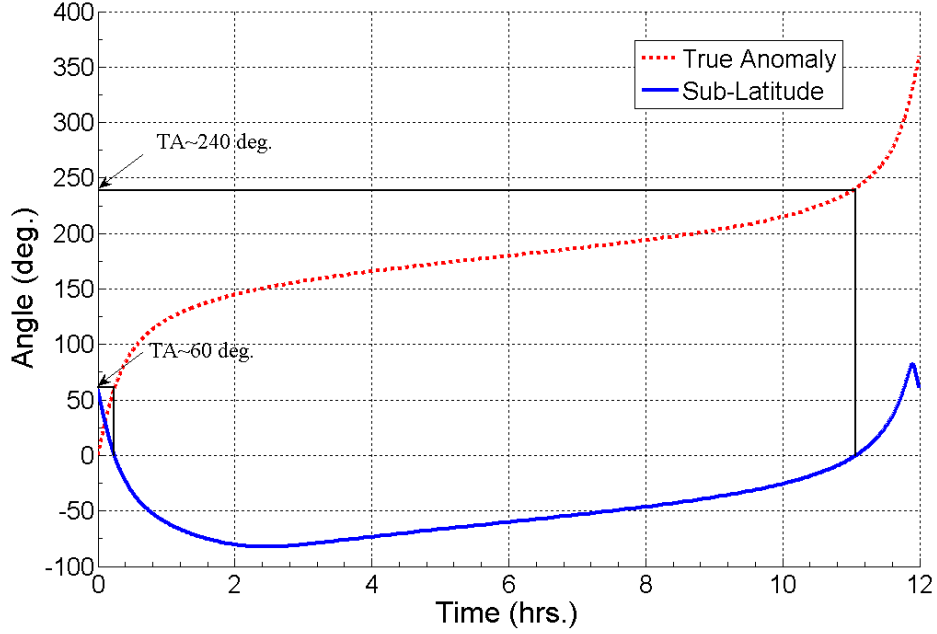


Figure 4. Spacecraft True Anomaly (TA) and Sub-Spacecraft Latitude Versus Time of a Typical Science Orbit.

The hot-pole configuration is implemented when the true anomaly of Mercury, v_{φ} , falls within, $I_{hp} = \{I_1 \cup I_2 : I_1 \in [260, 300] \text{ and } I_2 \in [80, 120]\}$, where values are given in degrees. When $v_{\varphi} \in I_{hp}$, the body axes of the spacecraft can take on two distinct orientations. If the true anomaly of the spacecraft $v_{sc} \in [-120, 60]$, then the $\hat{\mathbf{k}}^{hp1}$ -axis of the body frame, designated as $\hat{\mathbf{k}}^{hp1}$, points in the direction of Mercury's south pole. A vector parallel to Mercury's north pole in the J2000 frame, φ_{NP} , yields the unit vector $\hat{\mathbf{u}}_{\varphi_{NP}} = \varphi_{NP} / |\varphi_{NP}|$. The coordinate frame is described by the following equations:

$$\begin{aligned}
 \hat{\mathbf{k}}^{hp1} &= -\hat{\mathbf{u}}_{\varphi_{NP}} \\
 \hat{\mathbf{i}}^{hp1} &= -\hat{\mathbf{u}}_{\odot/sc} \times \hat{\mathbf{k}}^{hp1} \\
 \hat{\mathbf{j}}^{hp1} &= \hat{\mathbf{k}}^{hp1} \times \hat{\mathbf{i}}^{hp1}
 \end{aligned} \tag{15}$$

In this case, the sunshade, lying in the $-\hat{\mathbf{j}}^{hp1}$ direction, points in the approximate direction of the Sun (Figure 5).

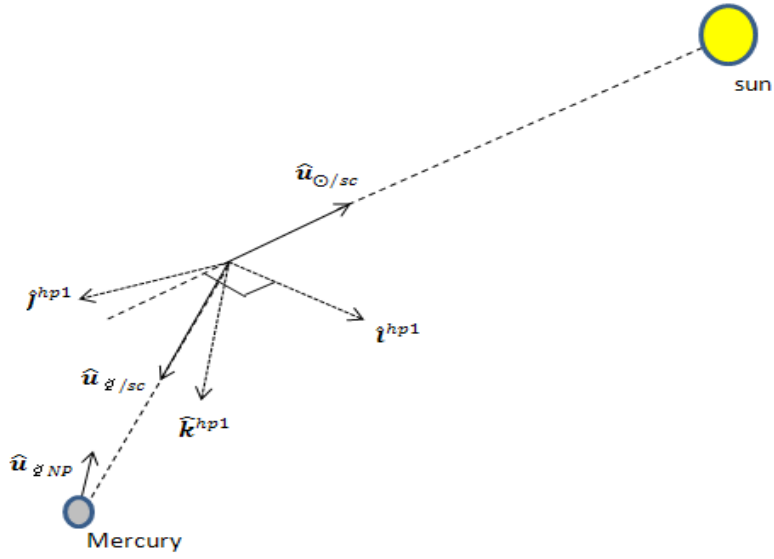


Figure 5. The $\hat{\mathbf{i}}^{hp1}, \hat{\mathbf{j}}^{hp1}, \hat{\mathbf{k}}^{hp1}$ -Frame with Respect to Mercury and the Sun.

The direction cosine matrix from the body frame to the J2000 frame is

$$C_{\text{body}/\text{J2000}}^{/hp1} = [\hat{\mathbf{i}}^{/hp1} \quad \hat{\mathbf{j}}^{/hp1} \quad \hat{\mathbf{k}}^{/hp1}]. \quad (16)$$

If $\nu_{sc} \in [60, 240]$, then the $\hat{\mathbf{k}}^{hp2}$ -axis of the body frame, $\hat{\mathbf{k}}^{hp2}$, points in the direction of Mercury's north pole. The coordinate frame is constructed such that the $-\hat{\mathbf{j}}^{hp2}$ direction points approximately in the direction of the Sun (Figure 6).

$$\begin{aligned} \hat{\mathbf{k}}^{hp2} &= \hat{\mathbf{u}}_{\varphi NP} \\ \hat{\mathbf{i}}^{hp2} &= -\hat{\mathbf{u}}_{\odot/sc} \times \hat{\mathbf{k}}^{hp2} \\ \hat{\mathbf{j}}^{hp2} &= \hat{\mathbf{k}}^{hp2} \times \hat{\mathbf{i}}^{hp2} \end{aligned} \quad (17)$$

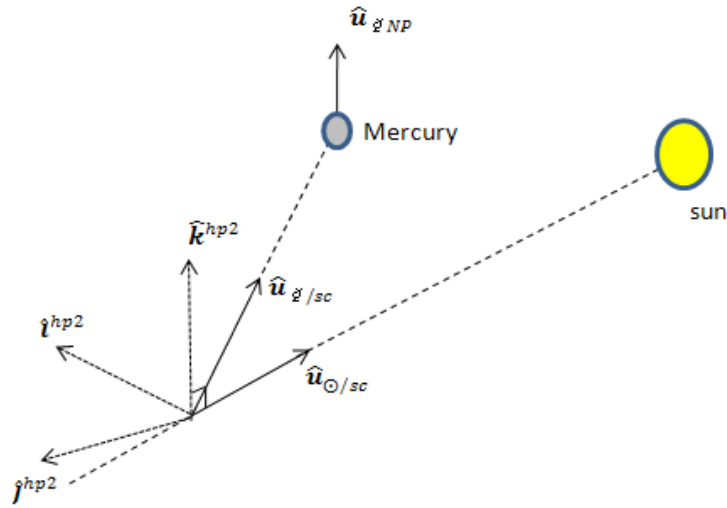


Figure 6. The $\hat{i}^{hp2}, \hat{j}^{hp2}, \hat{k}^{hp2}$ -Frame with Respect to Mercury and the Sun.

The direction cosine matrix is

$$C_{\text{body}/J2000}^{/hp2} = [\hat{i}^{/hp2} \quad \hat{j}^{/hp2} \quad \hat{k}^{/hp2}]. \quad (18)$$

RESULTS

SRP Versus Albedo-IR

The albedo-IR pressure is generally at least one order of magnitude less than SRP except when the groundtrack approaches the subsolar point. By rescaling the SRP acceleration, Lucchesi and Iafolla² estimate that the SRP force on the European Space Agency's BepiColombo Mercury Planetary Orbiter can be expected to be approximately 30 times that from Mercury albedo. Because MESSENGER has a highly eccentric science orbit ($e \sim 0.74$) with a much larger semi-major axis, the ratio is expected to fluctuate substantially. Figure 7 shows SRP and albedo-IR acceleration over a one-day propagation at the beginning of the science orbit phase.

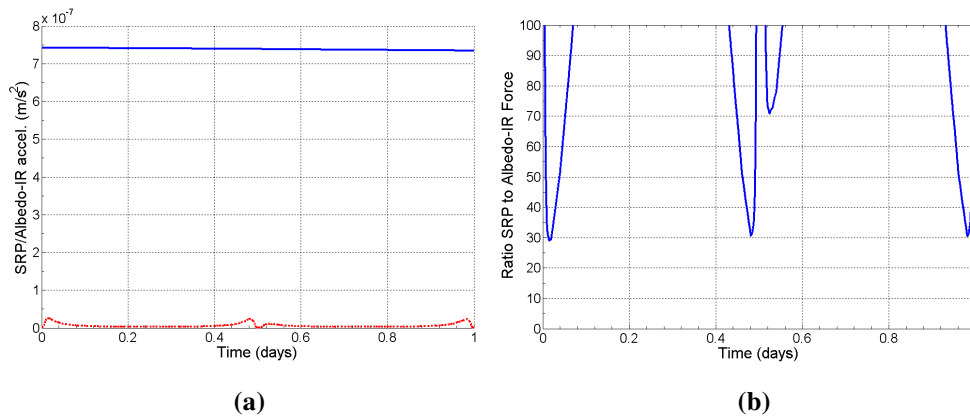


Figure 7. (a) SRP (Solid Blue Line) and Albedo-IR (Red Dashed Line) Acceleration Versus Time. (b) Ratio of SRP to Albedo-IR Acceleration Over Approximately Two Orbital Periods.

During this time period, it is expected that the maximum albedo-IR pressure will occur in the near spacecraft true anomaly values of $\pm 90^\circ$. These are the regions where sizeable areas of Mercury's sunlit surface are in view at a relatively close distance. Minima will occur near periherm and apherm. At periherm, the spacecraft is at a low altitude ($\sim 200\text{--}500$ km) with the majority of Mercury's lit surface blocked from view. The black lines on Mercury's limb in Figures 8c and 8d show the regions of Mercury's surface in view of the spacecraft.

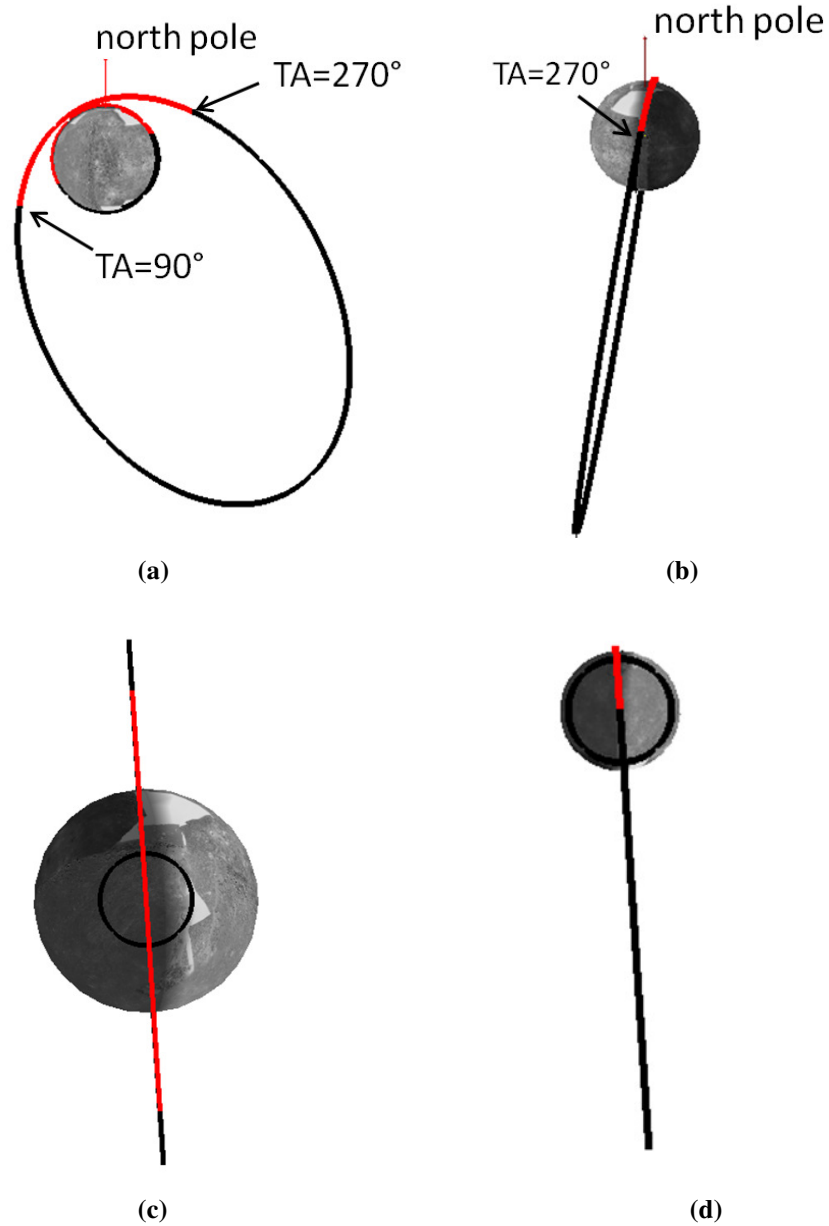


Figure 8. (a and b) Front and Edge-On Views of the Science Orbit after Orbit Insertion. (c and d) Spacecraft at True Anomalies of 0° and 90° , Respectively. Black Lines Enclose Areas of Mercury's Surface in View of the Spacecraft.

The albedo-IR accelerations on the spacecraft over one orbital period are displayed in Figure 9. The plot confirms that the acceleration peaks at true anomaly values in the vicinity of $\pm 90^\circ$ and attains minima and periapsis and apoapsis.

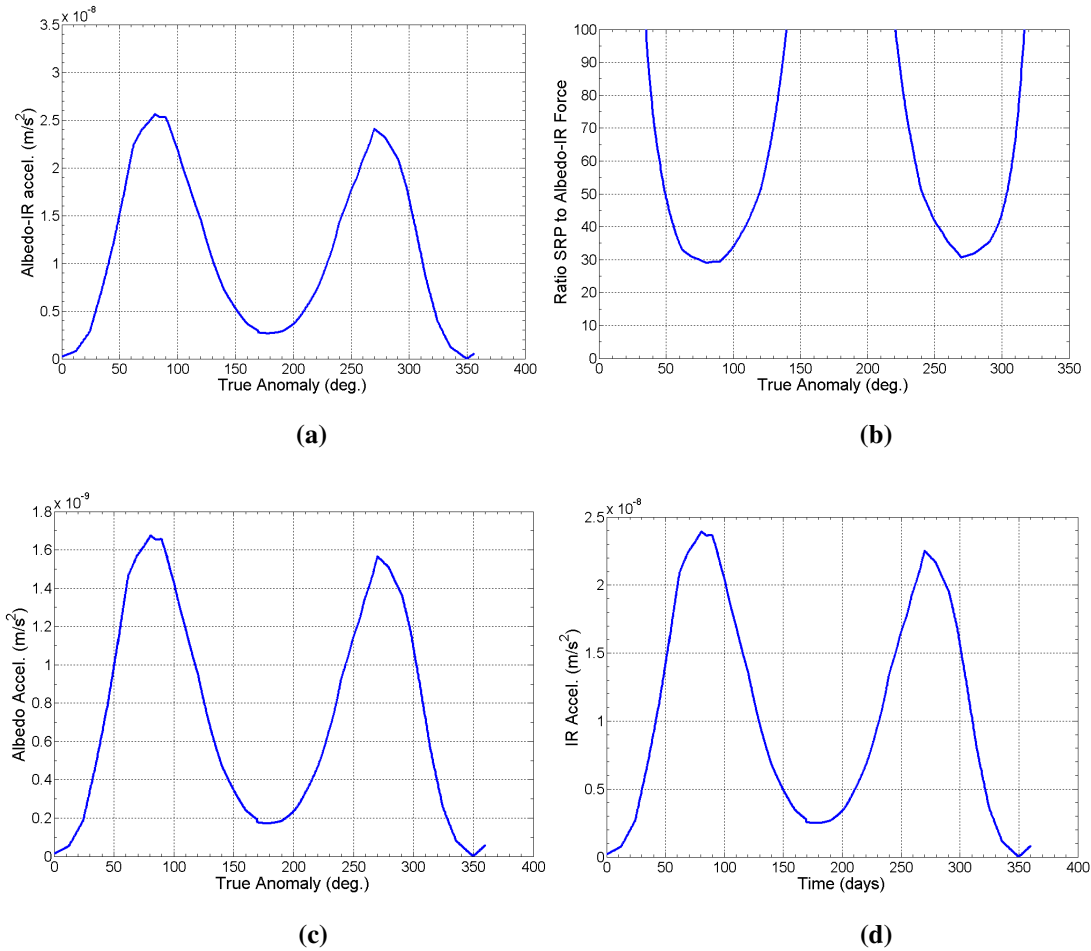


Figure 9. (a) Albedo-IR Acceleration Versus Spacecraft True Anomaly. (b) Ratio of SRP to Albedo-IR Acceleration Versus True Anomaly. (c and d) Albedo and IR Acceleration Versus Spacecraft True Anomaly.

Throughout the Mercury year, the angular momentum vector of the orbit shifts with respect to the vector from Mercury to the Sun. Thus, the frequency of the peaks of the albedo-IR acceleration evolves with the precession of the orbit. Figure 10 shows the change in orientation and lighting conditions of the science orbit. The highest albedo-IR forces will occur approximately three-quarters into Mercury's year. Here the spacecraft flies over the subsolar point at a spacecraft true anomaly of 90° .

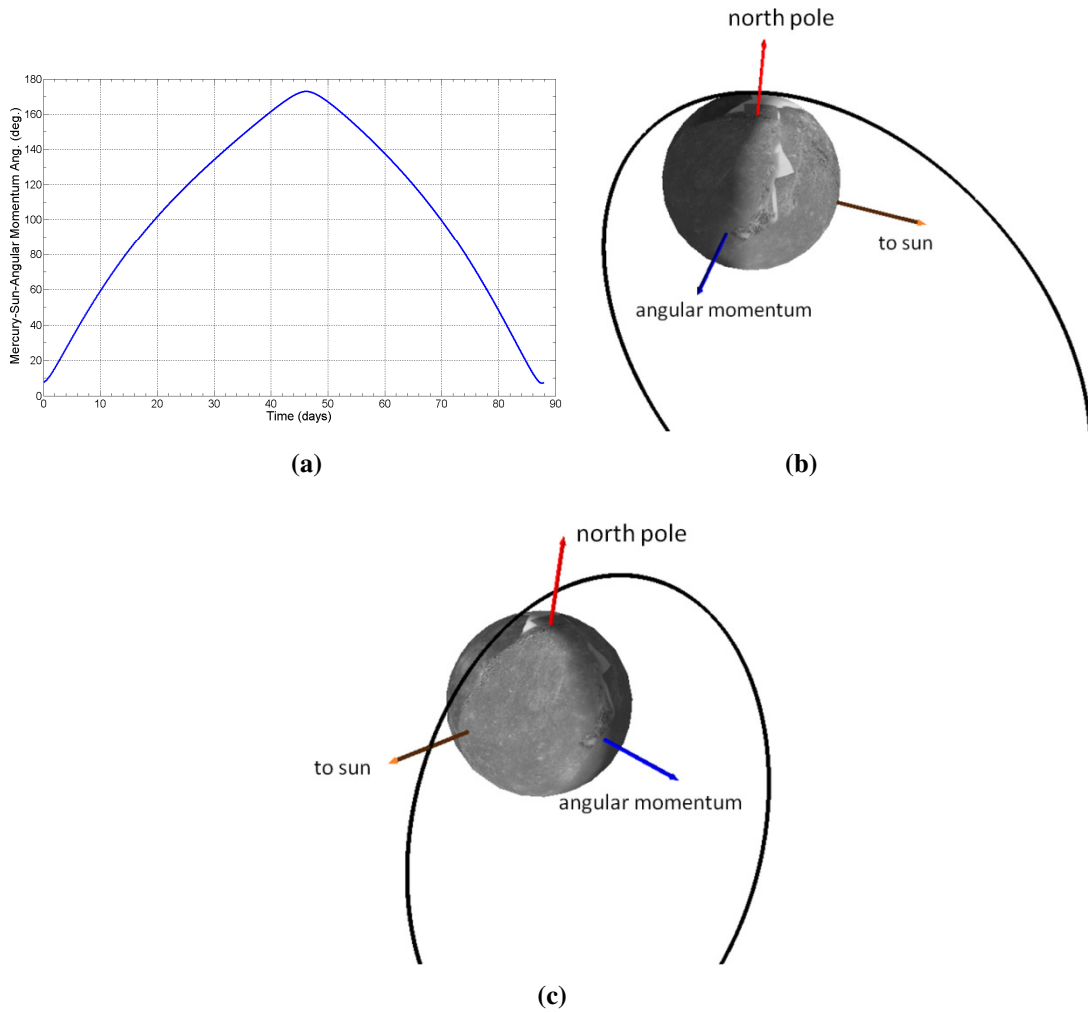


Figure 10. (a) Angle Between Mercury to Sun and Spacecraft Angular Momentum Vector Over a Mercury Year. (b) Science Orbit Geometry After a Quarter Mercury Year. (c) Science Orbit Geometry After Three-Quarters of a Mercury Year.

Accelerations due to SRP and albedo-IR over a typical science orbit approximately one-quarter into Mercury's year are shown in Figure 11. A single maximum is attained at a spacecraft true anomaly of near 270° . Here the acceleration due to albedo-IR reaches the same order of magnitude as SRP acceleration.

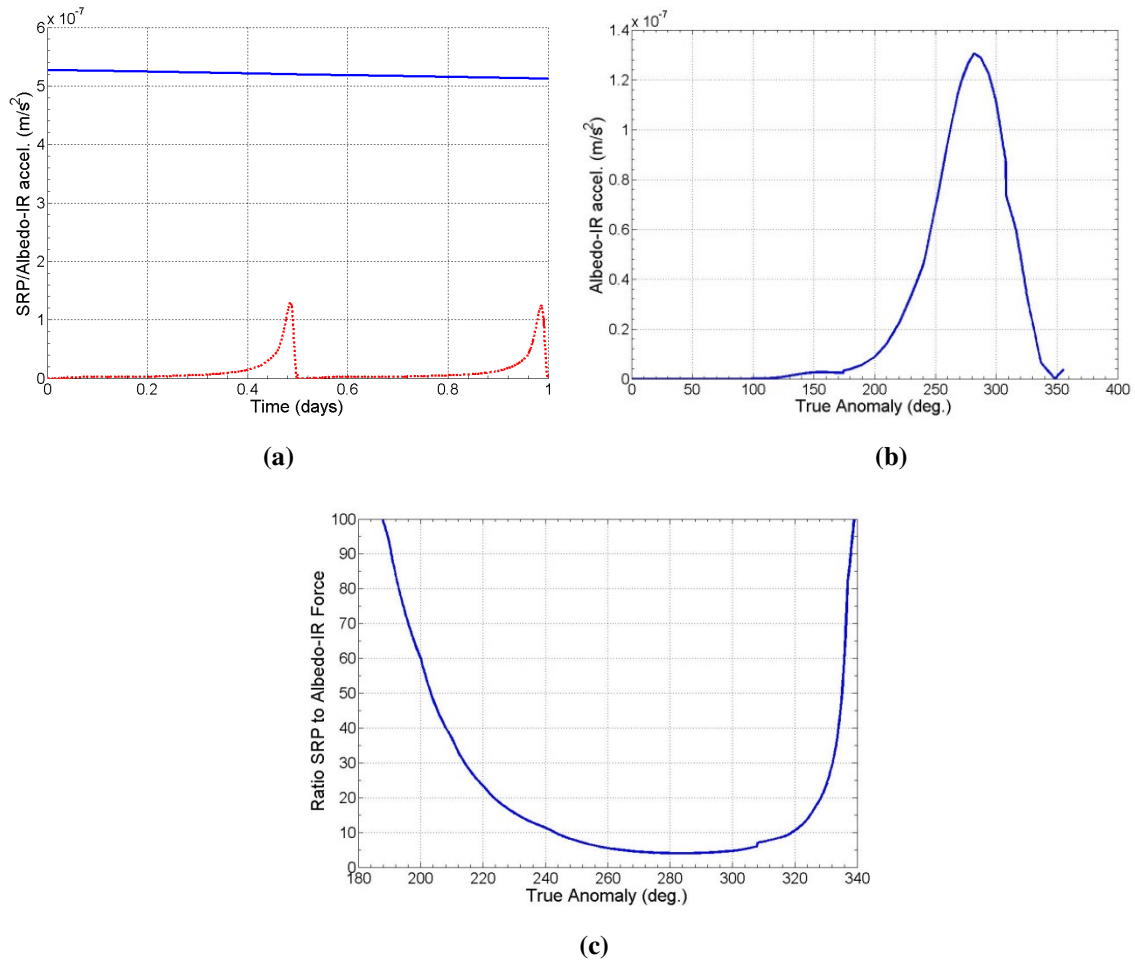


Figure 11. (a) SRP and Albedo-IR Accelerations over Approximately Two Orbits. (b) Albedo-IR Acceleration Versus True Anomaly. (c) Ratio of SRP to Albedo-IR Force Versus True Anomaly.

At three-quarters of a Mercury year, the accelerations due to albedo-IR surpass SRP for a true anomaly range of 355° – 95° (Figure 12). The intense conditions result from the spacecraft passing over the sub-solar point at a spacecraft true anomaly of 90° , which corresponds to a lower altitude than 270° true anomaly. Additionally, SRP has decreased because Mercury is closer to aphelion than the previous case.

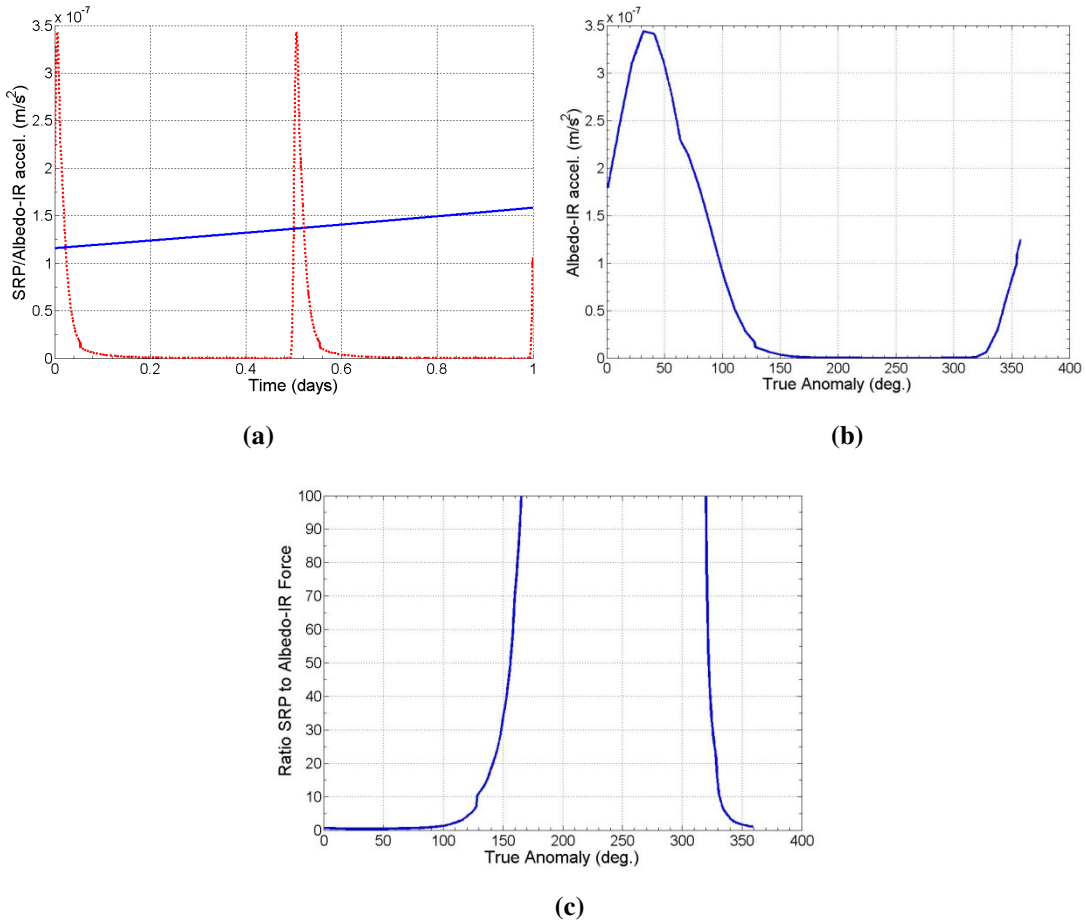


Figure 12. (a) SRP and Albedo-IR Accelerations over Approximately Two Orbits. (b) Albedo-IR Acceleration Versus True Anomaly. (c) Ratio of SRP to Albedo-IR Force Versus True Anomaly.

Orbit Evolution

Two 88-day simulations were performed. The first utilized the full force model excluding the albedo-IR perturbation, and the second used the full force model including albedo-IR. Figure 13 shows the difference in semi-major axis, inclination, and eccentricity between the two models. It is immediately evident that over a typical mission lifetime, the perturbation has a negligible effect on the qualitative properties of the orbit. Therefore, even in the harsh thermal environment of the inner solar system, albedo-IR perturbations are not necessary for science planning and maneuver design.

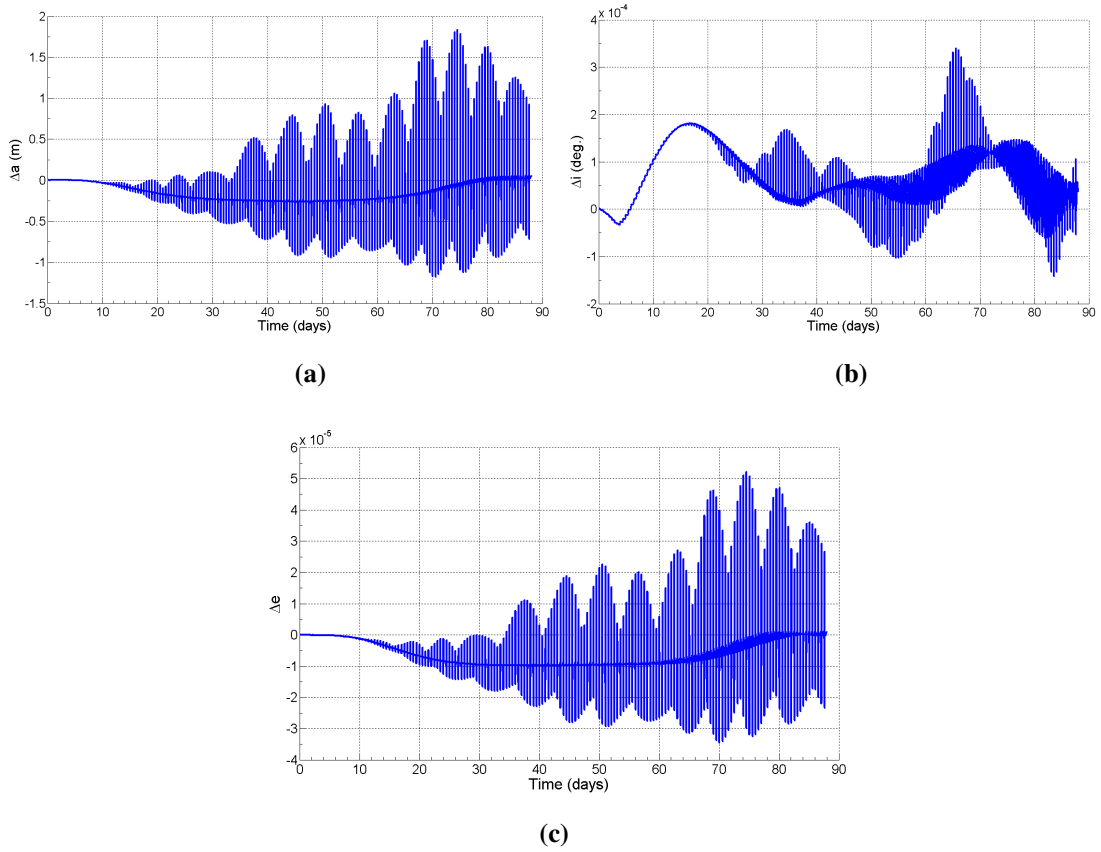
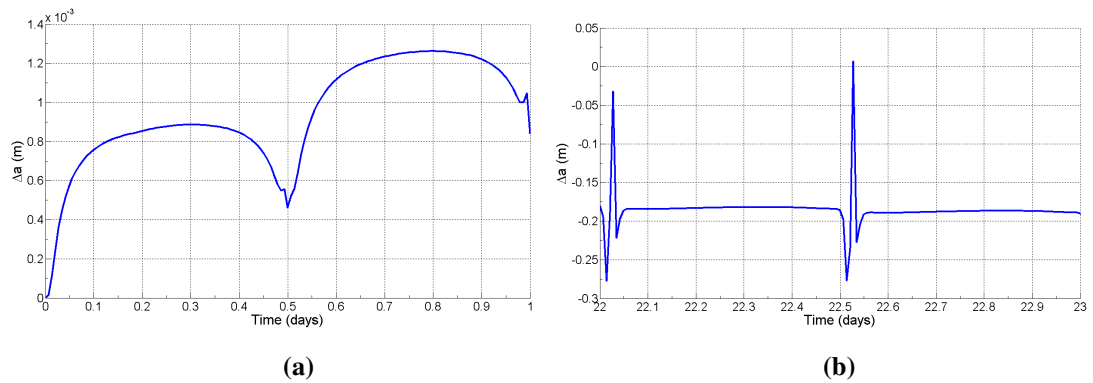
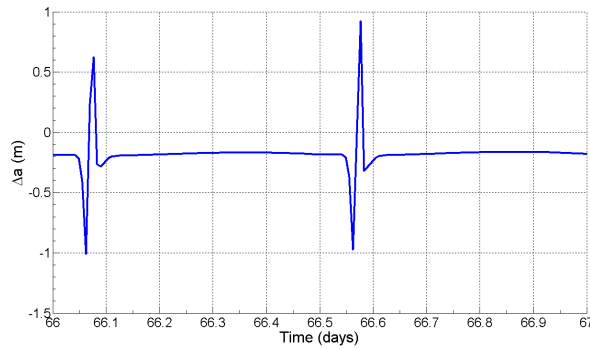


Figure 13. (a–c) Difference in Semi-Major Axis, Inclination, and Eccentricity Versus Time Due to the Albedo-IR Perturbation.

By comparing Figures 7a and 14a, the signal of the albedo-IR force can clearly be seen. Evident throughout the simulation, its amplitude grows larger with time.



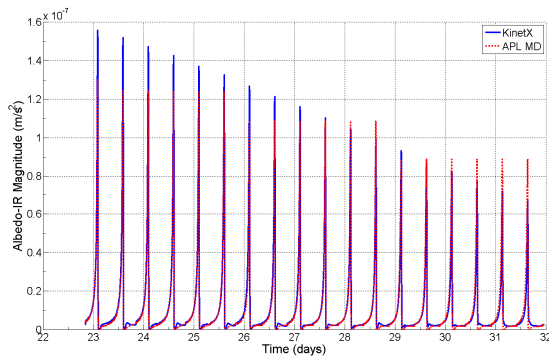


(c)

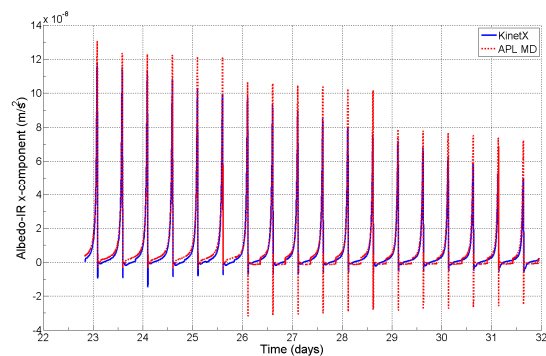
Figure 14. (a–c) Difference in Semi-Major Axis, Inclination, and Eccentricity Versus Time Due to the Albedo-IR.

Independent Comparison

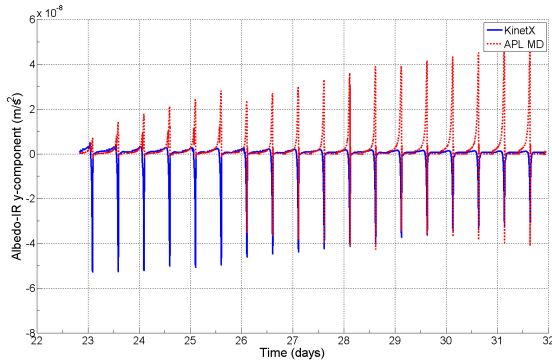
The attitude is adjusted on the basis of updated science and operation plans throughout the orbital phase of the mission. The attitude history will generally not follow the simplistic rules necessary for this study. Moreover, spacecraft material properties and assumptions related to Mercury’s surface radiance add more uncertainty to the model. Therefore, an independent comparison with data obtained from the navigation team at KinetX, Inc., was used to test the combined effects on the albedo-IR accelerations due to these error sources. The acceleration and material properties of the spacecraft are estimated from tracking data by KinetX. Figure 15 shows consistency in the magnitude and x -component of the acceleration, with noticeable inconsistencies in the y - and z -components.



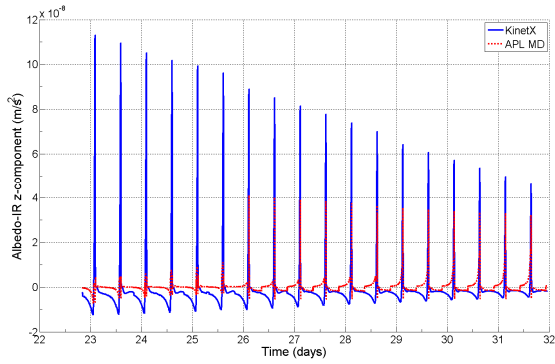
(a)



(b)



(c)



(d)

Figure 15. (a–d) Albedo-IR Acceleration Magnitude, x -, y -, and z -Components, Respectively, Supplied by The Johns Hopkins University Applied Physics Laboratory (APL) and KinetX. Time Is Indexed as Days Past Mercury Orbit Insertion.

The consistency in the magnitude continues until near the end of the first Mercury year of the orbital phase. A partial history is displayed in Figure 16.

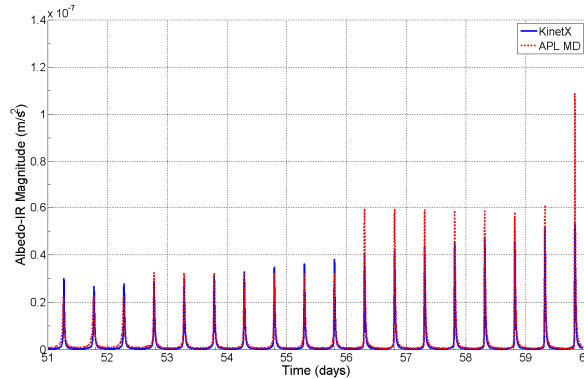


Figure 16. APL- and KinetXGenerated Albedo-IR Acceleration Magnitude.

CONCLUSIONS

The magnitude of the albedo-IR accelerations generated by the MESSENGER mission design team shows close agreement with values estimated by the navigation team, on the basis of tracking data. This result verifies that, independent of attitude, the assumptions made during this effort did not induce sizeable errors. Additionally, it demonstrates that the estimation methods employed by the navigation team show agreement with the model outlined in this paper. However, there are large discrepancies in the forces in the x - and z -directions due to the assumption made for spacecraft attitude necessary for this study. These differences could result in qualitative differences in the drift of the orbital elements and will require further analysis. The magnitudes of the drifts, along with the precision of science and navigation requirements, indicate that inclusion of an albedo-IR model for mission planning is not necessary over the duration of the mission.

ACKNOWLEDGMENT

The authors would like to thank the MESSENGER navigation team at KinetX, Inc., especially Tony Taylor, for providing their estimates for the albedo-IR accelerations.

REFERENCES

- ¹ J. V. McAdams, R. W. Farquhar, A. H. Taylor, and B. G. Williams, “MESSENGER Mission Design and Navigation.” *Space Sci. Rev.* 131, pp. 219–246, 2007.
- ² D. M. Lucchesi and V. Iafolla, “The Non-Gravitational Perturbations Impact on the BepiColombo Radio Science Experiment and the Key Role of the ISA Accelerometer: Direct Solar Radiation and Albedo Effects.” *Celestial Mech. Dyn. Astron.*, 96, pp. 99–127, 2006.
- ³ C. J. Ercol and A. G. Santo, “Determination of Optimum Thermal Phase Angles at Mercury Perihelion for an Orbiting Spacecraft.” *29th International Conference on Environmental Systems*, Society of Automotive Engineers, Tech. Paper Ser., paper 1999-01-21123, 10 pp., Denver, CO, July 12–15, 1999.
- ⁴ D. L. Domingue, F. Vilas, G. M. Holsclaw, J. Warell, N. R. Izenberg, S. L. Murchie, B. W. Denevi, D. T. Blewett, W. E. McClintock, B. J. Anderson, and M. Sarantos, “Whole-Disk Spectrophotometric Properties of Mercury: Synthesis of MESSENGER and Ground-Based Observations.” *Icarus*. 209, pp. 101–124, 2010.